Radiation dose estimation using preclinical imaging with ^{124}I-metaiodobenzylguanidine (MIBG) PET

Chang-Lae Lee
Department of Radiology and Biomedical Imaging, UCSF Physics Research Laboratory, University of California, San Francisco, San Francisco, California 94143 and Department of Radiological Science and Research Institute of Health Science, Yonsei University, Wonju 220-710, Korea

Hilla Wahnishe and George A. Sayre
Department of Radiology and Biomedical Imaging, UCSF Physics Research Laboratory, University of California, San Francisco, San Francisco, California 94143

Hyo-Min Cho and Hee-Joung Kim
Department of Radiology and Biomedical Imaging, UCSF Physics Research Laboratory, University of California, San Francisco, San Francisco, California 94143 and Department of Radiological Science and Research Institute of Health Science, Yonsei University, Wonju 220-710, Korea

Miguel Hernandez-Pampaloni, Randall A. Hawkins, Shorouk F. Dannoon, and Henry F. VanBrocklin
Department of Radiology and Biomedical Imaging, University of California, San Francisco, San Francisco, California 94143

Melissa Itsara
Department of Pediatrics, University of California, San Francisco, San Francisco, California 94143

William A. Weiss
Department of Neurology, University of California, San Francisco, San Francisco, California 94143

Xiaodong Yang and Daphne A. Haas-Kogan
Department of Radiation Oncology, Helen Diller Family Comprehensive Cancer Center, University of California, San Francisco, San Francisco, California 94143

Katherine K. Matthay
Department of Pediatrics, University of California, San Francisco, San Francisco, California 94143

Youngho Seo[a)]
Department of Radiology and Biomedical Imaging, UCSF Physics Research Laboratory, University of California, San Francisco, San Francisco, California 94143; Department of Radiation Oncology, Helen Diller Family Comprehensive Cancer Center, University of California, San Francisco, San Francisco, California 94143; and Joint Graduate Group in Bioengineering, University of California, San Francisco/Berkeley, San Francisco, California 94143

(Received 4 May 2010; revised 28 July 2010; accepted for publication 29 July 2010; published 20 August 2010)

Purpose: A pretherapy ^{124}I-metaiodobenzylguanidine (MIBG) positron emission tomography (PET)/computed tomography (CT) provides a potential method to estimate radiation dose to normal organs, as well as tumors prior to ^{131}I-MIBG treatment of neuroblastoma or pheochromocytoma. The aim of this work was to estimate human-equivalent internal radiation dose of ^{124}I-MIBG using PET/CT data in a murine xenograft model.

Methods: Athymic mice subcutaneously implanted with NB1691 cells that express high levels of human norepinephrine transporter (n=4) were imaged using small animal microPET/CT over 96 h (approximate imaging time points: 0.5, 2, 24, 52, and 96 h) after intravenous administration of 3.07–4.84 MBq of ^{124}I-MIBG via tail vein. The tumors did not accumulate ^{124}I-MIBG to a detectable level. All four animals were considered as control and organ radiation dosimetry was performed. Volumes of interest were drawn on the coregistered CT images for thyroid, heart, lung, liver, kidney, and bladder, and transferred to PET images to obtain pharmacokinetic data. Based on tabulated organ mass distributions for both mice and adult male human, preclinical pharmacokinetic data were extrapolated to their human-equivalent values. Radiation dose estimations for different age groups were performed using the OLINDA|EXM software with modified tissue weighting factors in the recent International Commission on Radiological Protection (ICRP) Publication 103.

Results: The mean effective dose from ^{124}I-MIBG using weighting factors from ICRP 103 to the adult male was estimated at 0.25 mSv/MBq. In different age groups, effective doses using values

from ICRP 103 were estimated as follows: Adult female: 0.34, 15-yr-old: 0.39 mSv/MBq, 10-yr-old: 0.58 mSv/MBq, 5-yr-old: 1.03 mSv/MBq, 1-yr-old: 1.92 mSv/MBq, and newborn: 3.75 mSv/MBq. For comparison, the reported effective dose equivalent of ^{124}I-NaI for adult male (25% thyroid uptake, MIRD Dose Estimate Report No. 5) was 6.5 mSv/MBq.

Conclusions: The authors estimated human-equivalent internal radiation dose of ^{124}I-MIBG using preclinical imaging data. As a reference, the effective dose estimation showed that ^{124}I-MIBG would deliver less radiation dose than ^{124}I-NaI, a radiotracer already being used in patients with thyroid cancer.
[DOI: 10.1118/1.3480965]

Key words: neuroblastoma, metaiodobenzylguanidine (MIBG), iodine-124, PET, dosimetry

I. INTRODUCTION

Iodine-124 is an emerging radionuclide for imaging because iodination techniques are common in developing new tracers for noninvasive nuclear molecular imaging.[1,2] Unlike ^{123}I which is an excellent radioiodine for imaging using a single photon emission computed tomography, ^{124}I can be imaged using positron emission tomography (PET) for more accurate quantification of tracer distribution. In addition, when combined with ^{131}I therapy such as ^{131}I-NaI for thyroid cancer or ^{131}I-metaiodobenzylguanidine (MIBG) for neuroblastoma or pheochromocytoma, ^{124}I PET imaging currently is the best modality for pretherapy dosimetry because of its favorable characteristics such as whole-body tomographic capability from PET and a similar half-life (4.2 d) to ^{131}I (8.02 d). For pretherapy dosimetry of ^{131}I treatment, ^{131}I can be also used as an imaging agent; however, as an imaging agent, ^{131}I is not an ideal radiolabel because the gamma emission from ^{131}I (photopeak of 364 keV) is not efficiently collected by a typical gamma camera with high-energy collimators and 3/8 in. NaI(Tl) crystal.[3] Roughly 50% or more of photons from ^{131}I escape the scintillation crystal and the collimators, even if they are designed for high-energy radionuclides such as ^{131}I, causing high fractions of collimator septa penetration and scatters that greatly degrade image quality of ^{131}I scans.[3,4]

For these reasons, ^{124}I-NaI imaging and dosimetry for ^{131}I-NaI treatment of thyroid cancer has been studied in recent years.[5–13] There are also other ^{124}I-labeled radiotracers that have been studied for other types of diseases.[14–18] However, ^{124}I-MIBG has not been systematically studied in human subjects. Although there was a report of using ^{124}I-MIBG in a limited number of human adult subjects (n=2) with neural crest tumors[19] and animals,[20] children with neuroblastoma or patients with pheochromocytoma were never studied using ^{124}I-MIBG. A more efficiently labeled form of MIBG (no-carrier-added) is currently in clinical trials (Ultratrace, Molecular Insight Pharmaceuticals, Cambridge, MA). This technology allows more activity to be administered with less of the chemical MIBG and ensures that every molecule taken up by the human norepinephrine transporter (hNET) will carry a radioactive iodine molecule.

As ^{131}I-MIBG therapy becomes more common and of proven efficacy for neuroblastoma and pheochromocytoma,[21–23] ^{124}I-MIBG pretherapy imaging and dosimetry in these patients will improve efficacy and safety with individualized adjustment of activity administered. As a first step, we performed preclinical imaging with no-carrier-added ^{124}I-MIBG using animal models in order to assess expected radiation exposures to human subjects. Data extrapolation and radiation dose estimations for models of different age groups are presented. The data presented in this report will be critical components for the Food and Drug Administration (FDA)'s Investigational New Drug application approval.

II. METHODS AND MATERIALS

II.A. ^{124}I-MIBG and Animal Models

We have labeled ^{124}I (purchased from IBA Molecular, Louvain-la-Neuve, Belgium) with MIBG synthesized from precursors provided by Molecular Insight Pharmaceuticals (Cambridge, MA).[24–28] From the reversed phase high performance liquid chromatography spectral analysis, we observed radiochemical purity of >99%. For thyroid blocking, 0.374 mg/100 μL of aqueous solution of sodium iodide was administered intravenously to four athymic mice (weighing approximately 25 g each). The mice were implanted with NB1691 cells that express hNET. We originally intended to investigate the tumor uptake of ^{124}I-MIBG in these animals. However, the subcutaneous xenograft tumors in these animal models did not accumulate ^{124}I-MIBG to a detectable level, possibly due to the difference in tumor microenvironments between native tumors and xenograft tumors. Thus, all four mice were considered as normal control subjects, and radiation dosimetry studies followed.

II.B. Small animal PET/CT

A total of 3.07–4.84 MBq of ^{124}I-MIBG was administered to four mice via tail vein. Small animal PET combined with computed tomography (microPET/CT) was performed immediately after ^{124}I-MIBG administration. We used a dedicated PET docked with multimodality CT (Inveon, Siemens Healthcare, Malvern, PA) for all of our preclinical imaging studies. Each animal was followed for over 96 h by imaging five time points (0.5, 2, 24, 52, and 96 h). Mice were under anesthesia using isoflurane at 2% concentration.

In order to obtain reasonable image qualities, we applied two PET data acquisition durations. At 0.5, 2, 24, and 52 h

reference time points, the data were acquired over 3600 s, and at 96 h, 5400 s. For the 0.5 h reference time point, we used a dynamic acquisition technique to capture early pharmacokinetics of the tracer immediately after the tracer administration. Thus, the actual acquisition time was from 0 to 1 h continuously, making the midtime point as reference at 0.5 h. The durations for the dynamic acquisition were 10×10, 5×40, 1×300, and 5×600 s. The 2 h data were also divided into two 1800 s frames.

PET data acquired using a 250–650 keV energy window were reconstructed to a $128 \times 128 \times 159$ matrix with a voxel size of $0.776\,383 \times 0.776\,383 \times 0.796$ mm^3 using the 2D-ordered subsets expectation maximization reconstruction algorithm. The CT images were reconstructed into a $512 \times 512 \times 672$ matrix with an isotropic voxel size of $0.190\,684 \times 0.190\,684 \times 0.190\,684$ mm^3 using a Feldkamp CT reconstruction algorithm modified for x-ray cone beam. The reconstruction algorithms for both PET and CT were provided by the scanner manufacturer. The parameters for microCT were 120 rotation steps over 220°, continuous acquisition, 80 kVp tube voltage, 500 μA tube current, and 175 ms exposure.

Image display and analysis were performed using the AMIDE software package.[29] Volumes of interest (VOIs) were drawn on the coregistered CT images for thyroid, heart, lung, liver, kidney, and bladder, and transferred to PET images to obtain the pharmacokinetic data. Once transferred to PET images, VOIs were adjusted to include apparent partial volume spill-outs for organ uptake calculation. VOIs of the thyroid were drawn with the reference to thyroid ^{124}I-MIBG PET images because the size of the thyroid was anatomically too small to be localized on CT.

The animal organ % of injected activity (%IA) data were converted to those for a human using the percent kilogram per gram method of Kirschner *et al.*[30] The calculated percent injected activity per gram of organ (%IA/g) for the organs in mice was extrapolated to uptake in organs of a 73.7 kg male adult.

In this method, the human %IA/organ is given as in Ref. 31

$$\left(\frac{\%\mathrm{IA}}{\mathrm{organ}}\right)_{\mathrm{human}} = \left[\left(\frac{\%\mathrm{IA}}{g_{\mathrm{organ}}}\right)_{\mathrm{animal}} \times (\mathrm{kg}_{\mathrm{TBweight}})_{\mathrm{animal}}\right] \times \left(\frac{g_{\mathrm{organ}}}{\mathrm{kg}_{\mathrm{TBweight}}}\right)_{\mathrm{human}}. \quad (1)$$

The calculated %IA/organ in the human organs was fitted with exponential biokinetic functions and integrated to obtain the number of disintegrations for source organs using the OLINDA|EXM (version 1.1) software.[32] The same software was used to estimate the effective dose in different age groups. The extracted organ masses and fractions for our radiation dose estimations between mouse and adult male are shown in Table I. The values of mouse organ masses and fractions were extracted from the standard Hui *et al.* model.[33,34]

TABLE I. Fractions of the total body mass of a reference adult male human (73 700 g) and mouse (25 g).

	Mouse		Human	
Organ	Mass (g)	Fraction	Mass (g)	Fraction
Thyroid	0.06	0.0024	20.7	0.0003
Heart	0.12	0.0048	316	0.0043
Lung	0.15	0.0060	1000	0.0136
Liver	1.05	0.0420	1910	0.0259
Kidney	0.27	0.0106	299	0.0041
Bladder	0.09	0.0036	47.6	0.0006

II.C. Dosimetric calculations

OLINDA|EXM software output is the radiation dose per unit of administered activity (mSv/MBq) in each organ and the total body, as well as effective dose (ED) and effective dose equivalent.[32,35] Inputs to OLINDA|EXM are either residence times themselves (uCi h/uCi, Bq h/Bq) or %IA/organ from which residence times are computed via exponential curve fits. The OLINDA phantoms are adjusted accordingly for different age groups from newborns to human adults. The time-activity-curves, expressed as percent injected activity per weight of tissue or percent injected activity of tissue (%IA/organ), were generated for the organs of interest. Effective dose was estimated for different age groups using the tissue weighting factors defined in the International Commission on Radiological Protection (ICRP) Publication 103 (Ref. 36) as well as the values in the ICRP Publication 60.[37] The current version of OLINDA|EXM (version 1.1) uses the ICRP Publication 60 tissue weighting factors.

III. RESULTS

Figure 1 shows selected slices of axial, coronal, and sagittal views of microPET/CT images from ^{124}I-MIBG from one of the animals included in our calculations. The five time points over 96 h show typical kinetics of ^{124}I-MIBG uptake

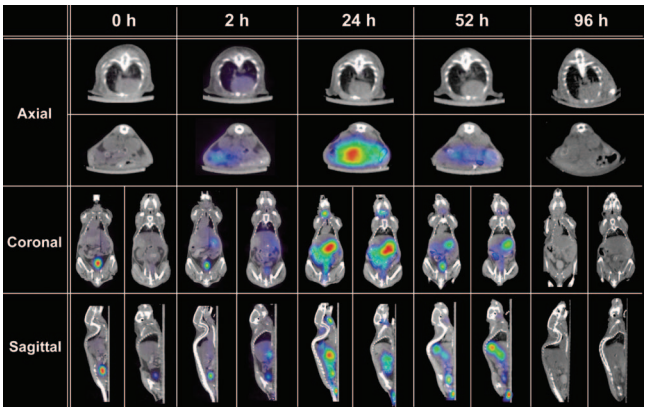

FIG. 1. Representative axial, coronal, and sagittal PET/CT views of ^{124}I-MIBG in a mouse. The images were acquired at 0.5, 2, 24, 52, and 96 h after intravenous injection of ^{124}I-MIBG. Lu=Lung; He=Heart; Li=Liver; Ki=Kidney; Bl=Bladder; and Th=Thyroid.

TABLE II. Biodistribution of ^{124}I-MIBG on mice at different time points (% IA/g). Values are expressed as %IA/g, mean ± standard error of the mean.

Time (h)	Thyroid	Heart	Lung	Liver	Kidney	Bladder
0	24.00 ± 3.89	20.88 ± 4.07	15.44 ± 4.86	13.06 ± 0.94	9.75 ± 1.05	242.51 ± 37.66
2	41.42 ± 5.08	19.98 ± 3.70	14.46 ± 2.83	11.64 ± 1.34	9.29 ± 1.32	124.41 ± 30.68
24	73.47 ± 3.10	10.75 ± 0.75	9.42 ± 1.13	7.36 ± 2.22	7.39 ± 1.47	69.44 ± 23.12
52	46.77 ± 9.44	7.43 ± 1.43	7.49 ± 1.82	4.77 ± 0.90	5.67 ± 0.66	79.34 ± 33.78
96	32.04 ± 5.72	2.81 ± 0.34	4.58 ± 1.56	2.94 ± 0.83	1.27 ± 0.36	21.24 ± 4.85

patterns. High uptake is found in the heart and bladder before the 2 h time point and thyroid uptake is heightened after the 24 h time point. Uptake in liver, kidneys, and lungs decreased continuously over time; however, the percent liver and lung uptake remained relatively high when compared to uptake in other organs even at the 96 h time point mostly due to their large fractions of organ masses. Table II lists the mean %IA/g values in each reported organ of mice. The %IA/g values were calculated by the fractions of activity in each organ (%IA) divided by organ masses in g (e.g., 0.12 g for heart in Table I).

Figure 2 illustrates extrapolated human-equivalent percent injected activity (%IA/organ) data in heart, thyroid, bladder, kidney, liver, and lung. The values shown in Fig. 2 are averaged across all four mice. The %IA/organ values show the expected patterns of pharmacokinetics. Since the thyroid was blocked from ^{124}I-MIBG by sodium iodide, the uptake in the thyroid was minimized. This process mimics the clinical situation in which patients are given potassium iodide (KI) as a thyroid-blocking agent.

The estimated equivalent dose to the organs and total body, and effective dose, for the reference adult male are summarized in Table III. The mean effective dose to the adult male was estimated to be 0.25 mSv/MBq. The highest mean equivalent dose was in the thyroid, at 2.343 mSv/MBq. Calculated effective doses for the different age groups are shown in Table IV. Effective dose values were higher in female than in male and are higher in the younger subjects than in the older subjects as expected.

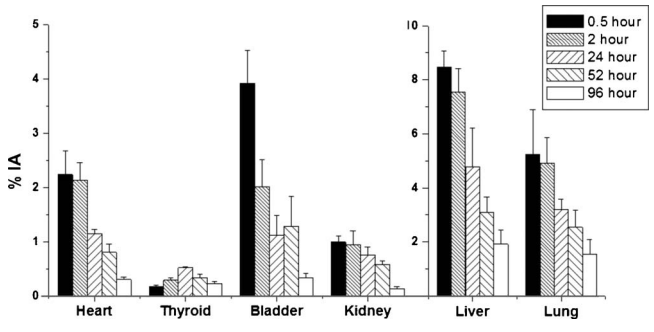

FIG. 2. Mean percent injected activity and standard error of the mean for ^{124}I-MIBG uptake in heart, thyroid, bladder, kidney, liver, and lung. Data are expressed as the extrapolated human-equivalent uptake values (%IA/organ).

IV. DISCUSSION

We have performed internal radiation dosimetry of ^{124}I-MIBG using microPET/CT in mice for normal organs with extrapolation to human-equivalent radiation dose values. Our results show that ^{124}I-MIBG PET is a feasible imaging modality for pretherapy dosimetry and the future possibility of its use for the prediction of tumor dose as well. The tissue weight factors extrapolation method [Eq. (1)] from mice to humans was based on preclinical imaging data. Therefore, the results are estimates of human absorbed dose since this method has uncertainties associated with extrapo-

TABLE III. Estimated equivalent doses and effective dose from ^{124}I-MIBG in reference adult male human. Values are expressed as mean ± standard error of the mean.

Target organ	Dose estimate	
	mSv/MBq	rem/mCi
Adrenals	0.117 ± 0.014	0.434 ± 0.052
Brain	0.038 ± 0.012	0.141 ± 0.046
Breasts	0.064 ± 0.012	0.235 ± 0.044
Gallbladder wall	0.141 ± 0.018	0.521 ± 0.065
LLI wall	0.064 ± 0.017	0.238 ± 0.063
Small intestine	0.069 ± 0.015	0.257 ± 0.056
Stomach wall	0.076 ± 0.014	0.282 ± 0.051
ULI wall	0.074 ± 0.014	0.275 ± 0.050
Heart wall	0.449 ± 0.035	1.663 ± 0.130
Kidneys	0.316 ± 0.038	1.170 ± 0.141
Liver	0.472 ± 0.112	1.750 ± 0.414
Lungs	0.428 ± 0.101	1.585 ± 0.370
Muscle	0.061 ± 0.013	0.226 ± 0.048
Ovaries	0.067 ± 0.017	0.249 ± 0.063
Pancreas	0.106 ± 0.014	0.392 ± 0.050
Red marrow	0.062 ± 0.012	0.230 ± 0.045
Osteogenic cells	0.075 ± 0.019	0.277 ± 0.071
Skin	0.042 ± 0.010	0.155 ± 0.037
Spleen	0.074 ± 0.014	0.273 ± 0.052
Testes	0.049 ± 0.014	0.182 ± 0.053
Thymus	0.082 ± 0.015	0.304 ± 0.055
Thyroid	2.343 ± 0.306	8.663 ± 1.129
Urinary bladder wall	0.462 ± 0.066	1.710 ± 0.245
Uterus	0.084 ± 0.019	0.310 ± 0.069
Total body	0.080 ± 0.012	0.295 ± 0.046
Effective dose (ICRP 60)	0.248 ± 0.021	0.918 ± 0.078
Effective dose (ICRP 103)	0.252 ± 0.021	0.932 ± 0.078

TABLE IV. Mean effective dose in different age groups for ^{124}I-MIBG extrapolated from animal data.

Age	Mass (g)	Effective dose (mSv/MBq)	
		ICRP 60	ICRP 103
Adult male	73 700	0.248	0.252
Adult female	57 000	0.348	0.342
15-yr-old	56 840	0.381	0.388
10-yr-old	33 200	0.568	0.578
5-yr-old	19 800	1.032	1.027
1-yr-old	9720	1.926	1.918
Newborn	3600	3.637	3.752

lation methods.[38] In our study, we also compared the effective dose estimates of ^{124}I-MIBG to effective doses reported for commonly known radiotracers (Table V).[39] The most significant finding from this comparison was that the estimated effective dose value of ^{124}I-MIBG was nearly ten times smaller than that of ^{124}I-NaI. Such discovery is important because ^{124}I-NaI is already used clinically at selected research centers.[6,7,9,10,40] The difference in effective dose values is primarily due to the thyroid blocking, which is performed for ^{124}I-MIBG studies, but not for ^{124}I-NaI studies. The ratio of estimated effective dose of ^{124}I-NaI to that of ^{124}I-MIBG (6.5/0.25) is comparable to the reported effective dose ratios of ^{123}I-NaI to ^{123}I-MIBG (0.12/0.019) and ^{131}I-NaI to ^{123}I-MIBG (11.0/0.21). The significant difference in effective doses between NaI and MIBG compounds primarily results from the different patterns of the two radiotracers. While the iodide anion will be taken up in the thyroid, the iodinated MIBG is specifically taken up by sympathetically innervated tissue (such as salivary gland) or tissue with the organic cation transporter (such as liver).[41]

The 0.25 mSv/MBq radiation dose estimated for ^{124}I-MIBG is significantly smaller than that of ^{124}I-NaI (6.5 mSv/MBq). However, this estimated dose is tenfold higher than that of ^{123}I-MIBG (0.019 mSv/MBq). Hence, as a diagnostic imaging agent that is used to identify MIBG-avid tumors, ^{124}I-MIBG may not be an ideal choice despite the quantitative ability of PET. For this reason, ^{124}I-MIBG PET should be administered at low doses especially for small children, and the best indication of ^{124}I-MIBG would be as a pretherapy dosimetry tool before ^{131}I-MIBG treatment for which the pretherapy radiation dose can be considered negligible by comparison. Particularly in younger pediatric patients, when ^{124}I-MIBG is used for pretherapy dosimetry of ^{131}I-MIBG treatment of neuroblastoma, the activity administered should be considered carefully. For example, for children under 5 years old, the estimated effective radiation dose is 1.03 mSv/MBq from ^{124}I-MIBG. In this case, if 18.5 MBq (0.5 mCi) of ^{124}I-MIBG is administered, the radiation exposure is estimated at 19.1 mSv, which is already approximately two thirds of effective dose from 555 MBq (15 mCi) administration of ^{18}F-flurodeoxyglucose (FDG) for adult male, 33.3 mSv using the tabulated values listed in Table V. An 18.5 MBq administration may appear to be an insufficient amount of activity to achieve acceptable quality PET images. However, the current PET technologies feature improved sensitivity over previous generations due to increased fields of view, 3-D acquisition. The possibility of allowing relatively long acquisition time per bed, particularly for small children without a requirement for increasing the total acquisition time, will result in accurate data for dosimetric calculations.

TABLE V. Comparisons of reference adult male estimated effective dose between ^{124}I-MIBG and selected known radiotracers.

Tracers	Effective dose (mSv/MBq)
^{124}I-MIBG (est.)	0.25
^{124}I-NaI	6.50
^{123}I-MIBG	0.019
^{123}I-NaI	0.12
^{131}I-MIBG	0.21
^{131}I-NaI	11.0
^{18}F-FDG	0.03

Several issues limited the accuracy of the dose calculation method used. In order to estimate the radiation dose using small animal data with high accuracy, we need to pay careful attention to a few specific points. One limitation of this work is the broad range of mouse organ masses from different animals. The underestimation of radiation dose in small organs can be caused by the limited spatial resolution of the microPET scanner when imaging ^{124}I-labeled radiotracers. However, the estimates of average whole-body dose generally are not significantly affected by partial volume errors.[42] Identifying accurate boundaries of organs is another practical difficulty. In addition, the radiation dose estimate might change depending on how many time points were used to acquire the data, which generally affects the quality of curve-fitting procedures using biokinetic time-activity-curves.

We also considered the radiotracer excretion model in our radiation dosimetry based on the total activity changes in the whole body of mice over time. For all imaging time points, the entire body of mice was included in the PET/CT field of view for this calculation. Radiation dose estimates including our excretion model were compared against the published ^{131}I-MIBG (no-carrier-added) pharmacokinetic and dosimetry data in humans.[43] Although technologies of estimating the radiation dose are quite different (microPET data extrapolation from mouse to human versus two-view anterior-posterior scintigraphy, which lacks robust quantitative measurements of radiotracer distribution), our preclinical ^{124}I-MIBG data were able to predict reasonably precise radiation dose estimates for ^{131}I-MIBG in humans within 15% of ED difference (0.34 mSv/MBq using ^{124}I-MIBG mouse biodistribution data converted for human dose estimates of ^{131}I versus 0.28 mSv/MBq calculated using residence times of each organ reported in Coleman *et al.*[43] for no-carrier-added ^{131}I-MIBG). Residence times predicted by the preclinical data of ^{124}I-MIBG were also in general agreement with those reported in Coleman *et al.* (Table VI).

TABLE VI. Comparison of ^{131}I-MIBG residence times (data from Coleman *et al.*) in humans (Ref. 43) versus estimated ^{131}I-MIBG residence times extrapolated from 124I-MIBG microPET data (this manuscript).

	^{131}I-MIBG residence times (Coleman *et al.*)		Estimated ^{131}I-MIBG residence times from ^{124}I-MIBG microPET data	
	Mean (h)	Range (h)	Mean (h)	Range (h)
Thyroid	0.45	0.27–0.72	0.53	0.38–0.72
Heart	0.80	0.48–1.18	0.88	0.80–0.96
Lung	2.97	1.69–4.89	3.27	2.50–2.86
Liver	5.37	2.57–11.92	5.03	3.37–6.75
Kidney	1.18	0.75–2.30	0.56	0.47–0.64
Bladder	2.01	1.63–2.19	1.20	0.87–1.47
Brain	0.54	0.28–0.78	–	–
Salivary gland	1.10	0.68–1.85	–	–
Spleen	0.82	0.50–1.28	–	–
Tumors	0.92	0.25–2.09	–	–
Remainder	23.25	15.21–40.39	18.86	9.26–24.54
Total body	36.54	23.86–65.18	30.33	22.46–34.39

V. CONCLUSION

Radiation absorbed dose estimation for internally administered radiopharmaceuticals using preclinical models is critical when translating a new radiopharmaceutical or a new indication using an existing radiopharmaceutical into clinical trials. The dose estimates for ^{124}I-MIBG using small animal models in our report showed that ^{124}I-MIBG would deliver a significantly smaller radiation dose than ^{124}I-NaI, a radiotracer already being used in human subjects. Our data support the safety of using ^{124}I-MIBG in humans as long as a relatively small amount of radioactivity is used. For example, the range of 0.5–1 mCi administration would result in effective dose estimates of 19.1–38.1 mSv in the 5-yr-old model. Also, as our results showed, for very young pediatric patients, particularly under 5 years old (effective dose estimates over 1 mSv/MBq), ^{124}I-MIBG imaging should be used judiciously and mainly in conjunction with a planned ^{131}I-MIBG therapy dose, which would then make the pretherapy imaging dose negligible by comparison.

ACKNOWLEDGMENTS

The authors acknowledge the following funding supports: National Cancer Institute Grant No. K25 CA114254 (G.A.S. and Y.S.), National Cancer Institute Grant No.R01 CA102321 (W.A.W.), Designated Grant from V Foundation (K.K.M., D.A.H., M.I., W.A.W., and Y.S.), and Dougherty Foundation and Alex Lemonade Foundation (K.K.M.).

[a]Author to whom correspondence should be addressed. Electronic mail: youngho.seo@ucsf.edu

[1]D. Dingli, B. J. Kemp, M. K. O'Connor, J. C. Morris, S. J. Russell, and V. J. Lowe, "Combined I-124 positron emission tomography/computed tomography imaging of NIS gene expression in animal models of stably transfected and intravenously transfected tumor," Mol. Imaging Biol. **8**, 16–23 (2006).

[2]M. J. Welch, R. Laforest, and J. S. Lewis, "Production of non-standard PET radionuclides and the application of radiopharmaceuticals labeled with these nuclides," in Proceedings of the Ernst Schering Research Foundation Workshop, 2007, pp. 159–181.

[3]D. Autret, A. Bitar, L. Ferrer, A. Lisbona, and M. Bardies, "Monte Carlo modeling of gamma cameras for I-131 imaging in targeted radiotherapy," Cancer Biother. Radiopharm. **20**, 77–84 (2005).

[4]M. Monsieurs, B. Brans, K. Bacher, R. Dierckx, and H. Thierens, "Patient dosimetry for 131I-MIBG therapy for neuroendocrine tumours based on 123I-MIBG scans," Eur. J. Nucl. Med. Mol. Imaging **29**, 1581–1587 (2002).

[5]F. Capoccetti, B. Criscuoli, G. Rossi, F. Ferretti, C. Manni, and E. Brianzoni, "The effectiveness of 124I PET/CT in patients with differentiated thyroid cancer," Q. J. Nucl. Med. Mol. Imaging **53**, 536–545 (2009).

[6]R. F. Hobbs, R. L. Wahl, M. A. Lodge, M. S. Javadi, S. Y. Cho, D. T. Chien, M. E. Ewertz, C. E. Esaias, P. W. Ladenson, and G. Sgouros, "124I PET-based 3D-RD dosimetry for a pediatric thyroid cancer patient: Real-time treatment planning and methodologic comparison," J. Nucl. Med. **50**, 1844–1847 (2009).

[7]W. Jentzen, L. Freudenberg, E. G. Eising, W. Sonnenschein, J. Knust, and A. Bockisch, "Optimized 124I PET dosimetry protocol for radioiodine therapy of differentiated thyroid cancer," J. Nucl. Med. **49**, 1017–1023 (2008).

[8]H. T. Phan, P. L. Jager, A. M. Paans, J. T. Plukker, M. G. Sturkenboom, W. J. Sluiter, B. H. Wolffenbuttel, R. A. Dierckx, and T. P. Links, "The diagnostic value of 124I-PET in patients with differentiated thyroid cancer," Eur. J. Nucl. Med. Mol. Imaging **35**, 958–965 (2008).

[9]L. S. Freudenberg, W. Jentzen, R. Gorges, T. Petrich, R. J. Marlowe, J. Knust, and A. Bockisch, "124I-PET dosimetry in advanced differentiated thyroid cancer: Therapeutic impact," Nucl. Med. (Stuttgart) **46**, 121–128 (2007).

[10]G. Sgouros, K. S. Kolbert, A. Sheikh, K. S. Pentlow, E. F. Mun, A. Barth, R. J. Robbins, and S. M. Larson, "Patient-specific dosimetry for 131I thyroid cancer therapy using 124I PET and 3-dimensional-internal dosimetry (3D-ID) software," J. Nucl. Med. **45**, 1366–1372 (2004).

[11]W. Jentzen, R. Weise, J. Kupferschlager, L. Freudenberg, W. Brandau, R. Bares, W. Burchert, and A. Bockisch, "Iodine-124 PET dosimetry in differentiated thyroid cancer: Recovery coefficient in 2D and 3D modes for PET(/CT) systems," Eur. J. Nucl. Med. Mol. Imaging **35**, 611–623 (2008).

[12]L. S. Freudenberg, G. Antoch, R. Gorges, J. Knust, R. Pink, W. Jentzen, J. F. Debatin, W. Brandau, A. Bockisch, and J. Stattaus, "Combined PET/CT with iodine-124 in diagnosis of spread metastatic thyroid carcinoma: A case report," Eur. Radiol. **13**, L19–L23 (2003).

[13]S. M. Larson *et al.*, "PET scanning of iodine-124-3F9 as an approach to tumor dosimetry during treatment planning for radioimmunotherapy in a child with neuroblastoma," J. Nucl. Med. **33**, 2020–2023 (1992).

[14]H. G. Keen, B. A. Dekker, L. Disley, D. Hastings, S. Lyons, A. J. Reader, P. Ottewell, A. Watson, and J. Zweit, "Imaging apoptosis in vivo using 124I-annexin V and PET," Nucl. Med. Biol. **32**, 395–402 (2005).

[15]L. A. Diaz, Jr. *et al.*, "Imaging of musculoskeletal bacterial infections by [124I]FIAU-PET/CT," PLoS ONE **2**, e1007 (2007).

[16]G. Reischl, D. S. Dorow, C. Cullinane, A. Katsifis, P. Roselt, D. Binns,

and R. J. Hicks, "Imaging of tumor hypoxia with [124I]IAZA in comparison with [18F]FMISO and [18F]FAZA—First small animal PET results," J. Pharm. Pharm. Sci. **10**, 203–211 (2007).
[17]I. Verel, G. W. Visser, M. J. Vosjan, R. Finn, R. Boellaard, and G. A. van Dongen, "High-quality 124I-labelled monoclonal antibodies for use as PET scouting agents prior to 131I-radioimmunotherapy," Eur. J. Nucl. Med. Mol. Imaging **31**, 1645–1652 (2004).
[18]G. Sundaresan, P. J. Yazaki, J. E. Shively, R. D. Finn, S. M. Larson, A. A. Raubitschek, L. E. Williams, A. F. Chatziioannou, S. S. Gambhir, and A. M. Wu, "124I-labeled engineered anti-CEA minibodies and diabodies allow high-contrast, antigen-specific small-animal PET imaging of xenografts in athymic mice," J. Nucl. Med. **44**, 1962–1969 (2003).
[19]R. J. Ott, D. Tait, M. A. Flower, J. W. Babich, and R. M. Lambrecht, "Treatment planning for 131I-mIBG radiotherapy of neural crest tumours using 124I-mIBG positron emission tomography," Br. J. Radiol. **65**, 787–791 (1992).
[20]M. A. Moroz, I. Serganova, P. Zanzonico, L. Ageyeva, T. Beresten, E. Dyomina, E. Burnazi, R. D. Finn, M. Doubrovin, and R. G. Blasberg, "Imaging hNET reporter gene expression with 124I-MIBG," J. Nucl. Med. **48**, 827–836 (2007).
[21]S. Gonias, R. Goldsby, K. K. Matthay, R. Hawkins, D. Price, J. Huberty, L. Damon, C. Linker, A. Sznewajs, S. Shiboski, and P. Fitzgerald, "Phase II study of high-dose [131I]metaiodobenzylguanidine therapy for patients with metastatic pheochromocytoma and paraganglioma," J. Clin. Oncol. **27**, 4162–4168 (2009).
[22]K. K. Matthay, C. Panina, J. Huberty, D. Price, D. V. Glidden, H. R. Tang, R. A. Hawkins, J. Veatch, and B. Hasegawa, "Correlation of tumor and whole-body dosimetry with tumor response and toxicity in refractory neuroblastoma treated with (131)I-MIBG," J. Nucl. Med. **42**, 1713–1721 (2001).
[23]K. K. Matthay, G. Yanik, J. Messina, A. Quach, J. Huberty, S. C. Cheng, J. Veatch, R. Goldsby, P. Brophy, L. S. Kersun, R. A. Hawkins, and J. M. Maris, "Phase II study on the effect of disease sites, age, and prior therapy on response to iodine-131-metaiodobenzylguanidine therapy in refractory neuroblastoma," J. Clin. Oncol. **25**, 1054–1060 (2007).
[24]G. Vaidyanathan, D. J. Affleck, and M. R. Zalutsky, "No-carrier-added synthesis of a 4-methyl-substituted meta-iodobenzylguanidine analogue," Appl. Radiat. Isot. **62**, 435–440 (2005).
[25]G. Vaidyanathan and M. R. Zalutsky, "No-carrier-added meta-[123I]iodobenzylguanidine: Synthesis and preliminary evaluation," Nucl. Med. Biol. **22**, 61–64 (1995).
[26]G. Vaidyanathan, H. S. Friedman, S. T. Keir, and M. R. Zalutsky, "Localisation of [131I]MIBG in nude mice bearing SK-N-SH human neuroblastoma xenografts: Effect of specific activity," Br. J. Cancer **73**, 1171–1177 (1996).
[27]M. N. Gaze, R. J. Mairs, G. Vaidyanathan, and M. R. Zalutsky, "Synthesis of carrier-free 131I-meta-iodobenzyl-guanidine by novel routes to enhance therapeutic efficiency in neuroblastoma," Prog. Clin. Biol. Res. **385**, 347–353 (1994).
[28]G. D. Flux, M. J. Guy, P. Papavasileiou, C. South, S. J. Chittenden, M. A. Flower, and S. T. Meller, "Absorbed dose ratios for repeated therapy of neuroblastoma with I-131 mIBG," Cancer Biother. Radiopharm. **18**, 81–87 (2003).
[29]A. M. Loening and S. S. Gambhir, "AMIDE: A free software tool for multimodality medical image analysis," Mol. Imaging **2**, 131–137 (2003).
[30]A. S. Kirschner, R. D. Ice, and W. H. Beierwaltes, "Radiation dosimetry of 131I-19-iodocholesterol," J. Nucl. Med. **14**, 713–717 (1973).
[31]S. H. Waxler and M. Enger, "Organ weights and obesity in mice," J. Nutr. **54**, 209–214 (1954).
[32]M. G. Stabin, R. B. Sparks, and E. Crowe, "OLINDA/EXM: The second-generation personal computer software for internal dose assessment in nuclear medicine," J. Nucl. Med. **46**, 1023–1027 (2005).
[33]T. E. Hui, D. R. Fisher, J. A. Kuhn, L. E. Williams, C. Nourigat, C. C. Badger, B. G. Beatty, and J. D. Beatty, "A mouse model for calculating cross-organ beta doses from yttrium-90-labeled immunoconjugates," Cancer **73**, 951–957 (1994).
[34]W. H. Miller, C. Hartmann-Siantar, D. Fisher, M. A. Descalle, T. Daly, J. Lehmann, M. R. Lewis, T. Hoffman, J. Smith, P. D. Situ, and W. A. Volkert, "Evaluation of beta-absorbed fractions in a mouse model for 90Y, 188Re, 166Ho, 149Pm, 64Cu, and 177Lu radionuclides," Cancer Biother. Radiopharm. **20**, 436–449 (2005).
[35]V. Kersemans, B. Cornelissen, K. Bacher, K. Kersemans, H. Thierens, R. A. Dierckx, B. De Spiegeleer, G. Slegers, and J. Mertens, "In vivo evaluation and dosimetry of 123I-2-iodo-D-phenylalanine, a new potential tumor-specific tracer for SPECT, in an R1M rhabdomyosarcoma athymic mouse model," J. Nucl. Med. **46**, 2104–2111 (2005).
[36]"ICRP Publication 103: The 2007 Recommendations of the International Commission on Radiological Protection," Ann. ICRP **37** (2007).
[37]"ICRP Publication 60: Recommendation of the International Commission on Radiological Protection," Ann. ICRP **21** (1991).
[38]P. Luoto, I. Laitinen, S. Suilamo, K. Nagren, and A. Roivainen, "Human dosimetry of carbon-11 labeled N-butan-2-yl-1-(2-chlorophenyl)-N-methylisoquinoline-3-carboxamide extrapolated from whole-body distribution kinetics and radiometabolism in rats," Mol. Imaging Biol. **12**, 435–442 (2010).
[39]M. Stabin, J. Stubbs, and R. Toohey, *Radiation Dose Estimates for Radiopharmaceuticals* (Oak Ridge Institute for Science and Education, Oak Ridge, 1996).
[40]R. Gorges, G. Antoch, W. Brandau, L. S. Freudenberg, J. Knust, K. Dutschka, S. P. Muller, W. Jentzen, A. Bockisch, and J. Stattaus, "Combination PET/CT with 124I positron rays in metastatic follicular thyroid carcinoma," Nucl. Med. (Stuttgart) **41**, N68–N71 (2002).
[41]M. Bayer, Z. Kuci, E. Schomig, D. Grundemann, H. Dittmann, R. Handgretinger, and G. Bruchelt, "Uptake of mIBG and catecholamines in noradrenaline- and organic cation transporter-expressing cells: Potential use of corticosterone for a preferred uptake in neuroblastoma- and pheochromocytoma cells," Nucl. Med. Biol. **36**, 287–294 (2009).
[42]H. Liang, Y. Yang, K. Yang, Y. Wu, J. M. Boone, and S. R. Cherry, "A microPET/CT system for in vivo small animal imaging," Phys. Med. Biol. **52**, 3881–3894 (2007).
[43]R. E. Coleman, J. B. Stubbs, J. A. Barrett, M. de la Guardia, N. Lafrance, and J. W. Babich, "Radiation dosimetry, pharmacokinetics, and safety of ultratrace Iobenguane I-131 in patients with malignant pheochromocytoma/paraganglioma or metastatic carcinoid," Cancer Biother. Radiopharm. **24**, 469–475 (2009).